Coordinated multi-band angle insensitive selection absorber based on graphene metamaterials

ZHIYU BAO,[1] JICHENG WANG,[1,3] ZHENG-DA HU,[1] ALIAKSEI BALMAKOU,[2] SERGEI KHAKHOMOV,[2] YANG TANG,[1] AND CHENLIANG ZHANG[1,*]

[1]*School of Science, Jiangsu Provincial Research Center of Light Industrial Optoelectronic Engineering and Technology, Jiangnan University, 214122 Wuxi, China*
[2]*Department of Optics, Francisk Skorina Gomel State University, Sovetskaya Str. 104, 246019, Gomel, Belarus*
[3]*jcwang@jiangnan.edu.cn*
[*]zhangcl@jiangnan.edu.cn

Abstract: In this paper, we propose a tunable, multi-band, selective absorber composed of multiple layers. Each layer consisted of SiO_2/graphene/SiC, and a layer of silver was used as the ground plane of the entire structure. Simulation results show that we can passively and actively coordinate the resonant frequency of the perfect absorption peak by changing the geometric parameters of the array and the Fermi level of the graphene. The absorber is not sensitive to the angle of incidence and the direction of polarization. We propose a theoretical basis for the formation of multiple absorption peaks. The theoretical calculations are in good agreement with the simulation results. In addition, we simulated the three- and four-layer structures. The results show that in the terahertz (THz) band, composite structures of three and four layers can obtain three and four perfect absorption peaks, respectively. Our results provide new insights into the THz band of harmonizable multi-band absorbers that can be applied to THz imaging to coordinate sensors and other optoelectronic devices.

1. Introduction

Graphene, a new, two-dimensional material composed of carbon atoms with an atomic thickness, has various transmission phenomena unique to two-dimensional Dirac fermions [1] and remarkable optical properties [2]. Graphene has a broad absorbable frequency domain, which can be extended to THz and microwave regions due to its unique linear energy-momentum dispersion relationship [3–5]. Because plasma can control sub-wavelength-sized light and propagate on the surface of the material-thereby effectively and feasibly implementing nanophotonics-in recent years, surface plasma (SP) research has received increasing attention. The SP in graphene can be regarded as a collective oscillation of its surface electrons, and a certain energy and momentum are obtained by coupling with other energies to propagate on the surface of the material [6–8]. Therefore, utilizing the propagation characteristics of graphene SP can have many applications, including plasma-based graphene modulators [9–12] and sensors [13–15].

An electromagnetic (EM) absorber can disable light propagation channels such as reflection and scattering, allowing incident light to be absorbed at the operating frequency. It has great potential in many applications, such as solar photovoltaic cells and photo-detectors [16,17]. Early EM absorbers were created by W.W Salisbury and J. Jaumann to improve radar performance and hide other radar systems that operate primarily in the microwave band [18,19]. With the gradual emergence of metamaterials [20,21], the working range of EM absorbers has gradually expanded to THz and optical frequencies [22–25]. In 2008, C. M. Bingham et al. proposed a multi-resonator metamaterial consisting of one, two, and three unique sub-lattices with multi-resonant frequencies in the THz frequency domain [26].

Subsequently, X. Liu et al. proposed a space-dependent, supermaterial, perfect absorber that works in the mid-infrared region [27]. However, although some of the structures proposed in [28–31] can achieve multi-band absorption in the THz band, there are still some limitations-such as low absorption efficiency and an inability to achieve a single coordination of a certain resonant frequency.

In this paper, we propose a novel, multi-band, angle-insensitive selective absorber based on graphene. Its structure is composed of two layers. In each layer, a square ring monolayer graphene is present between the SiC substrate and the SiO$_2$ coating. There is also a silver ground plane that reflects EM waves. We simulated the proposed structure using the commercial finite element method (FEM) solver COMSOL Multiphysics. We analyzed the physical mechanism of selective absorption using the coupled mode theory (CMT). The COMSOL simulation results were in good agreement with the CMT numerical results. The results show that we can modulate the resonance frequency of the corresponding absorption peak by adjusting a certain layer of graphene separately. We can choose any two perfect absorption peaks in a relatively wide THz band by passively adjusting the structural parameters. Active coordination of perfect absorption can also be achieved by changing the Fermi level. Due to the structure's high degree of symmetry and the locality of the SP resonance, our perfect absorber is insensitive to both the incident angle and the polarization direction.

2. Structure and theoretical analysis

A three-dimensional structure of a graphene-based selective absorber is proposed in Fig. 1(a). The red arrows indicate the incident TM wave. The incident plane is the X-Z plane. The red cuboid represents silver with a thickness of d_2. The blue and the yellow cuboids represent SiC and SiO$_2$ layers respectively. In the THz range, the refractive index of SiC [32] can be expressed as n = $(7.634 + 3.026 \times \lambda^2 /(\lambda^2\text{-}175.2))^{1/2}$ and the dielectric constant of SiO$_2$ [33] can be estimated as ε_{SiO2} = 3.9 by static value. The single-layer graphene between the square rings is set to the surface current density in a COMSOL simulation because their thicknesses are too small.

In this paper, we use the Kubo formula to describe the surface conductivity of graphene layers [34–36]:

$$\sigma_{gra} = \sigma_{inter} + \sigma_{intra} = \frac{2e^2 k_B T}{\pi \hbar^2} \frac{i}{\omega + i/\tau} \ln\left[2\cos h(\frac{E_f}{2k_B T})\right]$$
$$+ \frac{e^2}{4\hbar^2}\left[\frac{1}{2} + \frac{1}{\pi}\arctan(\frac{\hbar\omega - 2E_f}{2k_B T}) - \frac{i}{2\pi}\ln\frac{(\hbar\omega + 2E_f)^2}{(\hbar\omega - 2E_f)^2 + 4(k_B T)^2}\right], \quad (1)$$

where σ_{inter} and σ_{intra} are expressed as the interband and intraband transition contributions, respectively. k_B, $\hbar$ and e represent the Boltzmann constant, reduced Plank constant, and electron charge, respectively. ω is the angular frequency of the incident radiation, E_f is a graphene Fermi energy level, τ is the electron-phonon relaxation time, and T is the ambient temperature. As we only consider highly doped graphene, we should take into account that $E_f \gg k_B T$ and $E_f \gg \hbar\omega$. At this time, the Kubo equation can be simplified to a Drude-like model [37–39]:

$$\sigma_{gra} = \frac{e^2 E_f}{\pi\hbar^2}\frac{i}{\omega + i/\tau}. \quad (2)$$

where E_f is set to 0.8eV, $\tau = \mu E_f/(ev2 F)$, μ and $v F$ represent the media carrier mobility and the graphene Fermi velocity, respectively. We set $\mu = 1 \times 10^4 cm^2 V^{-1} s^{-1}$ [40,41] and $v F = 1 \times 10^6 ms^{-1}$. As shown in Fig. 1(a), which simulates the structure of the design, the X-Z plane

serves as the incident plane of TM radiative, and the periodic boundary conditions are along the X and Y directions.
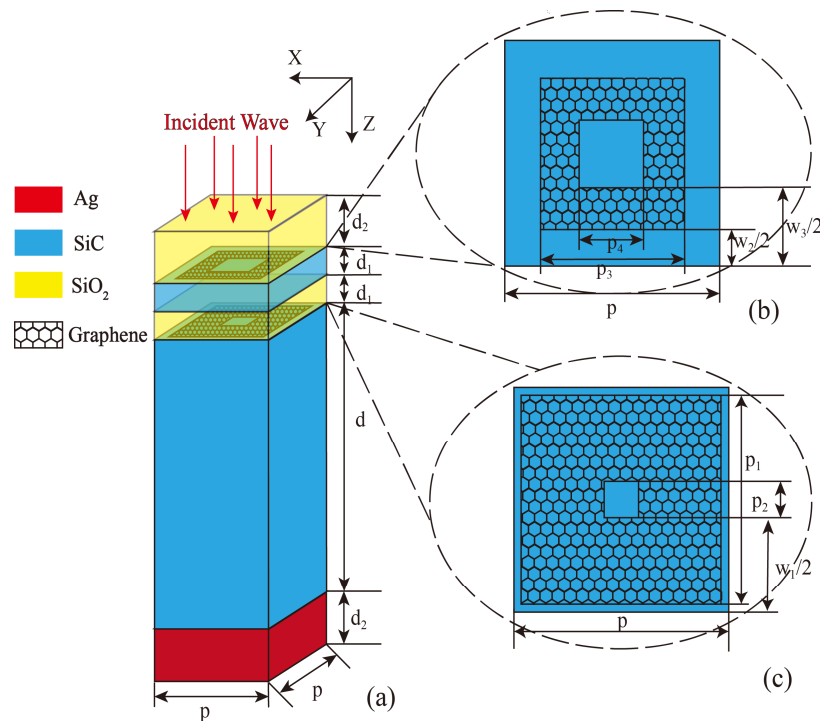

Fig. 1. (a) Three-dimensional diagram of the proposed structure; (b) Top graphene layer; and (c) Bottom graphene layer.

Figure 2(a) shows the dependence of the absorptance on frequency for the simulation structure (black curve), the structure with the bottom graphene layer only (red curve), and the structure with the top graphene layer only (blue curve). We have structural parameters for the absorber: $p = 1000$ nm, $d = 2000$ nm, $d_1 = 100$ nm, $d_2 = 200$ nm, $p_1 = 940$ nm, $p_2 = 140$ nm, $p_3 = 680$ nm, and $p_4 = 280$ nm. The proposed structure obtained two perfect absorption peaks at frequencies of 3.67 THz and 4.68 THz, while the structure with the bottom graphene layer only and the structure with the top graphene layer only reached the absorption peak at 3.67 THz and 4.68 THz, respectively.

Next, we will briefly explain the contribution of the top and lower graphene to the absorption spectrum of the proposed structure from the electric field distribution. Figures 2(b) and 2(d) show the electric field distribution of the top graphene and the bottom graphene at 3.67 THz. We can clearly observe that at an incident frequency of 3.67 THz, the electric field strength of the bottom graphene is much stronger than that of the top graphene. This indicates that the resonance absorption of the proposed structure at 3.67 THz is mainly due to the bottom graphene. Similarly, the electric field distribution of the top graphene and bottom graphene at 4.68 THz are shown in Figs. 2(c) and 2(e), and it can be clearly seen that the resonance absorption of the structure is mainly due to the top graphene.
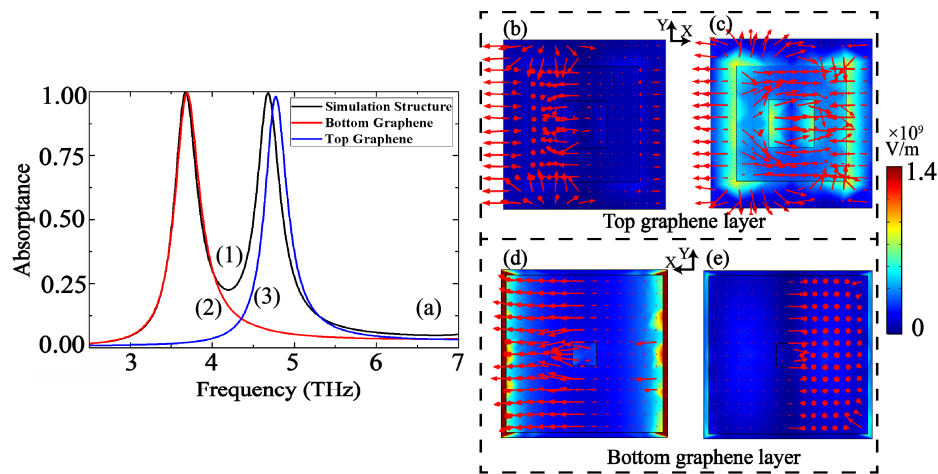
Fig. 2. (a) Absorptance vs. frequency for: (1) the entire simulated structure, (2) the structure with bottom graphene layer only (w/o the top layer), and (3) the structure with top graphene layer only (w/o the bottom layer); electric field distribution in: (b) and (c) the top graphene layer; and (d) and (e) the bottom graphene layer, when exciting at the resonant frequencies of 3.67 THz and 4.68 THz, respectively.

Now, we will use CMT to explain in detail the two peaks that appear in the absorption spectrum of the proposed structure. As shown in Fig. 3(a), the elements A_1 and element A_2 are considered two resonators that describe the coupling mechanism between the top graphene and the bottom graphene. The top graphene and the lower graphene are coupled to the incident light to form two absorption spectral modes, and then the two absorption spectral modes are coupled. This process can be regarded as the first coupling, as shown in Fig. 3(a). This series of processes takes place in Fig. 3(d) C-1. Then, as shown in Fig. 3(b), the coupled EM wave is reflected by silver and coupled again with the two layers of graphene. This process can be regarded as the second coupling, and the series of processes takes place in Fig. 3(d) C-2. After that, the coupled wave will be reflected by the bottommost SiC and silver substrate, and then coupled with the two layers of graphene to complete the third coupling, as shown in Fig. 3(c). This series of processes is shown in Fig. 3(d) C-3. As the number of times this happens increases, the coupling effect deteriorates. Moreover, the calculation process becomes increasingly complicated. To simplify the calculation process, we only consider the influence of C-1 and C-2 coupling on absorption. In Figs. 3(a)-3(c), "in" and "out" are used to describe the incident and outgoing radiation waves in the two modes, and the "+" and "-" are used to describe the direction of radiation propagation, where "+" is the direction of propagation of the incident wave and "-" is the direction of propagation of the reflected wave.
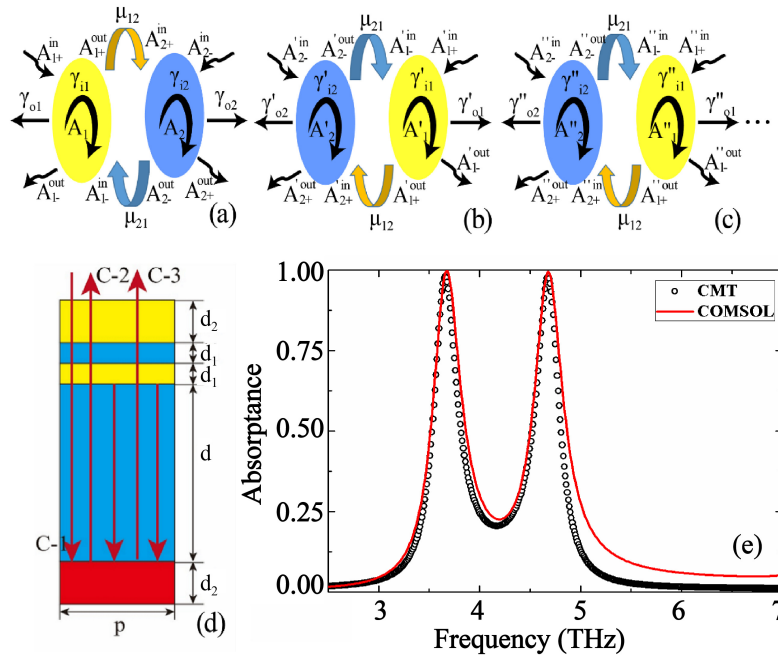
Fig. 3. (a)-(c) Representations of the equivalent CMT model of the simulation structure; (d) coupling effect illustrated for the simulation structure, and (e) absorptance vs. frequency diagrams obtained by CMT and COMSOL.

Therefore, the two oscillations mA_1 and mA_2 coupled for the first time, can be expressed as [42,43]:

$$\begin{pmatrix} rA_1 & -i\mu_{12} \\ -i\mu_{21} & rA_2 \end{pmatrix} \cdot \begin{pmatrix} mA_1 \\ mA_2 \end{pmatrix} = \begin{pmatrix} -\tau_{01}^{-1/2} & 0 \\ 0 & -\tau_{02}^{-1/2} \end{pmatrix} \cdot \begin{pmatrix} A_{1+}^{in} + A_{1-}^{in} \\ A_{2+}^{in} + A_{2-}^{in} \end{pmatrix}, \tag{3}$$

and the two oscillations of the second coupling, $mA'1$ and $mA'2$ can be expressed as:

$$\begin{pmatrix} rA_2' & -i\mu_{12} \\ -i\mu_{21} & rA_1' \end{pmatrix} \cdot \begin{pmatrix} mA_2' \\ mA_1' \end{pmatrix} = \begin{pmatrix} -\tau_{02}'^{-1/2} & 0 \\ 0 & -\tau_{01}'^{-1/2} \end{pmatrix} \cdot \begin{pmatrix} A_{2+}'^{in} + A_{2-}'^{in} \\ A_{1+}'^{in} + A_{1-}'^{in} \end{pmatrix}, \tag{4}$$

where: $rA1(2) = (i\omega - i\omega 1(2) - \gamma i1(2) - \gamma o1(2))$, $rA'1(2) = (i\omega - i\omega'1(2) - \gamma'i1(2) - \gamma'o1(2))$, ω is the angular frequency of the incident wave, $\omega 1(2)$ and $\omega'1(2)$ are the radiation mode angular frequencies of the first and second coupling, μ_{12} and μ_{21} are the radiation mode coupling coefficient $\gamma i1(2) = \tau$-1 $i1(2) = \omega 1(2)/(2Q i1(2))$ and $\gamma'i1(2) = \tau'$-1 $i1(2) = \omega'1(2)/(2Q i1(2))$ are the dacay rate due to the inherent loss of the first and second coupling, $\gamma o1(2) = \tau$-1 $o1(2) = \omega 1(2)/(2Q o1(2))$ and $\gamma'o1(2) = \tau'$-1 $o1(2) = \omega'1(2)/(2Q o1(2))$ are the decay rate due to power escaping into outside space in the first and second coupling, and $Q i1(2)$ and $Q o1(2)$ are the radiation mode quality factors related to internal loss or diffusion loss, respectively. The radiation mode quality factor of internal loss can be obtained through the complex refractive index of graphene: $Q i1(2) = \mathrm{Re}(n \, eff)/\mathrm{Im}(n \, eff)$, $n \, eff = \beta/k \, 0$. Simultaneously, $Q t1(2) = 1/Q$ $i1(2) + 1/Q o1(2)$, $Q t1(2) = f/\Delta f$ is the total quality factor of the radiation mode (where f is the resonant frequency and Δf expresses the full width at half of the maximum).

According to the law of conservation of energy, the two radiation modes satisfy the following relationship when first coupled:

$$A_{2+}^{in} = A_{1+}^{out} \cdot e^{i\theta}, A_{1-}^{in} = A_{2-}^{out} \cdot e^{i\theta}, \tag{5}$$

$$A_{1\pm}^{out} = A_{1\pm}^{in} - \tau_{01}^{-1/2} \cdot mA_1, A_{2\pm}^{out} = A_{2\pm}^{in} - \tau_{02}^{-1/2} \cdot mA_2, \tag{6}$$

and the two radiation modes satisfy the following relationship when coupled for the second time:

$$A_{1-}^{'in} = A_{2-}^{'out} \cdot e^{i\theta}, A_{2+}^{'in} = A_{1+}^{'out} \cdot e^{i\theta}, \tag{7}$$

$$A_{1\pm}^{'out} = A_{1\pm}^{'in} - \tau_{01}^{'-1/2} \cdot mA_1^{'}, A_{2\pm}^{'out} = A_{2\pm}^{'in} - \tau_{02}^{'-1/2} \cdot mA_2^{'}, \tag{8}$$

Because the incident wave is incident in the "+" direction during the first coupling, $A^{in} 2- = 0$; for the same reason, $A'^{in} 1+ = 0$ in the second coupling. At this point, we can get the expression of the transmission coefficient by combining formulas (3)-(8):

$$
\begin{aligned}
t &= \frac{A_{1-}^{'out}}{A_{1+}^{in}} = \frac{A_{1-}^{'out}}{A_{2-}^{in}} \cdot \frac{A_{2+}^{out}}{A_{1+}^{in}} \\
&= \Big\{ e^{i\theta} + \Big[\tau_{01}^{-1} r_{A_2} e^{i\theta} + \tau_{02}^{-1} r_{A_1} e^{i\theta} + (\tau_{01}\tau_{02})^{-1/2} e^{2i\theta} \chi_{A_1} \\
&\quad + (\tau_{01}\tau_{02})^{-1/2} \chi_{A_2} \Big] \cdot (r_{A_1} r_{A_2} - \chi_{A_1} \chi_{A_2})^{-1} \Big\} \\
&\quad \cdot \Big\{ e^{i\theta} + \Big[\tau_{02}^{'-1} r_{A_1^{'}} e^{i\theta} + \tau_{01}^{'-1} r_{A_2^{'}} e^{i\theta} + (\tau_{01}^{'}\tau_{02}^{'})^{-1/2} e^{2i\theta} \chi_{A_2^{'}} \\
&\quad + (\tau_{01}^{'}\tau_{02}^{'})^{-1/2} \chi_{A_1^{'}} \Big] \cdot (r_{A_1^{'}} r_{A_2^{'}} - \chi_{A_1^{'}} \chi_{A_2^{'}})^{-1} \Big\}
\end{aligned}
\tag{9}
$$

$$
\begin{aligned}
r &= \frac{A_{1-}^{out}}{A_{1+}^{in}} = \Big[\tau_{01}^{-1} r_{A_2} + \tau_{02}^{-1} r_{A_1} e^{2i\theta} + (\tau_{01}\tau_{02})^{-1/2} e^{i\theta} \chi_{A_1} \\
&\quad + (\tau_{01}\tau_{02})^{-1/2} \chi_{A_2} e^{i\theta} \Big] \cdot (r_{A_1} r_{A_2} - \chi_{A_1} \chi_{A_2})^{-1},
\end{aligned}
\tag{10}
$$

where

$$
\begin{aligned}
\chi_{A_{2(1)}} &= iu_{12(21)} + 2\sqrt{\tau_{01}\tau_{02}} \cdot e^{i\theta}, \\
\chi_{A_{2(1)}^{'}} &= iu_{12(21)} + 2\sqrt{\tau_{01}^{'}\tau_{02}^{'}} \cdot e^{i\theta}
\end{aligned}
\tag{11}
$$

Thus, the absorptance can be obtained from Eqs. (9) and (10):

$$A = 1 - |t|^2 - |r|^2. \tag{12}$$

Although we use a simplified CMT model, it is in good agreement with the simulation results obtained from the COMSOL model, as shown in Fig. 3(e).

3. Influences of parameter variations on absorption peak

In order to explore the absorption properties of the proposed structure, we calculated its absorption spectra under different parameters, as seen in Figs. 4(a) and 4(b), which show absorption spectra when the widths of the outer and inner rings of the bottom graphene are changed. When p_1 is increased from 900 nm to 960 nm, the left absorption peak shifts toward the low frequency direction, the range of motion is relatively large (from 4.08 THz to 3.33 THz), and both are perfectly absorbed. When w_1 is increased from 760 nm to 840 nm, the left absorption peak shifts toward the high frequency direction, the moving range is relatively small, and both are perfectly absorbed. In the process of changing p_1 and w_1, the resonance frequency and absorptance of the right absorption peaks remain unchanged. Figures 4(c) and 4(d) represent absorption spectra when the widths of the outer and inner rings of the top graphene are changed. When w_2 is increased from 280 nm to 360 nm, the right absorption peak

shifts toward the high frequency direction, the movement range is relatively small, and the absorption peak slightly decreases, but is still greater than 98%. When w_3 is increased from 680 nm to 760 nm, the right absorption peak shifts toward the high frequency direction, the range of motion is relatively large (from 4.42 THz to 4.68 THz), and the absorption peak gradually increases to achieve perfect absorption. In the process of changing w_2 and w_3, the resonance frequency and absorptance of the left absorption peaks remain unchanged. Figure 4(e) shows the absorption spectrum when changing the media carrier mobility of the graphene. When μ is increased from 1 m^2/Vs to 1.5 m^2/Vs, the peak of the absorption spectrum gradually decreases and the frequency corresponding to the absorption peak does not change.
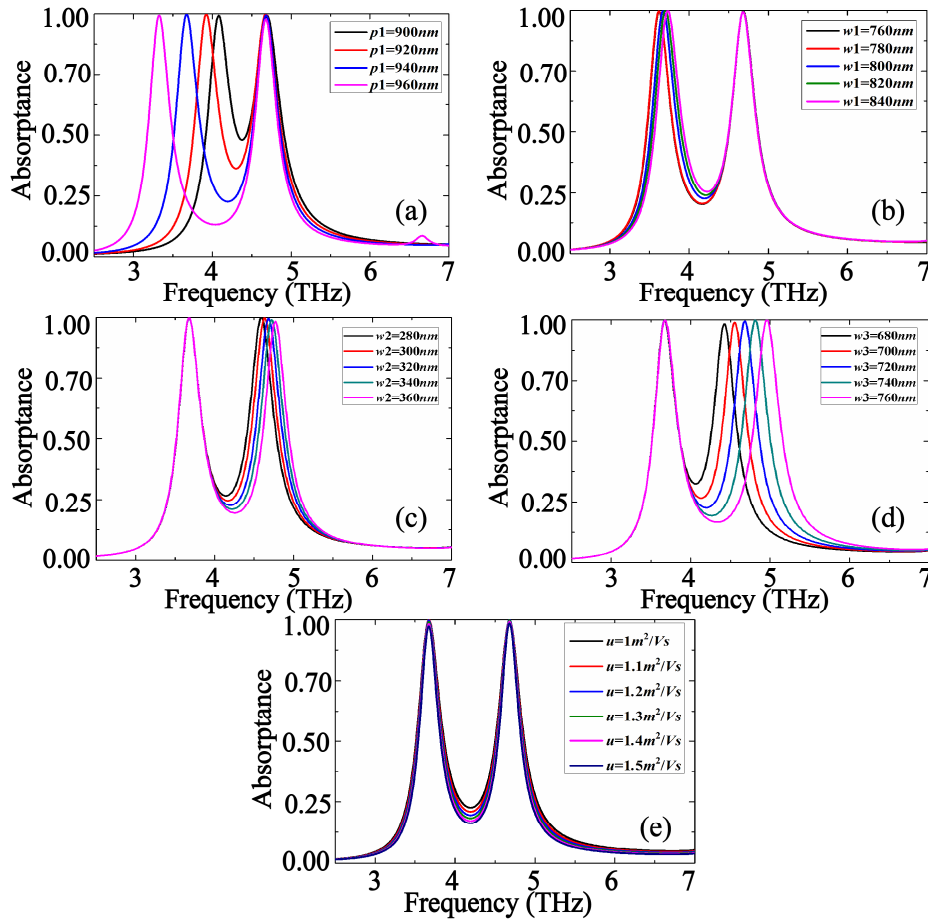

Fig. 4. (a)-(e) Absorption spectra after changing parameters p_1, w_1, w_2, w_3 and μ, respectively. Only one parameter is changed at a time. The original parameters are p_1 = 940 nm, w_1 = 800 nm, w_2 = 320 nm, w_3 = 720 nm, μ = 1m^2/Vs, $p_2 = p$-w_1, $p_3 = p$-w_2, $p_4 = p$-w_3.

As shown in Figs. 5(a) and 5(b) are TM wave incidence and TE wave incidence, respectively. For TM wave incidence, the absorptance of the proposed structure is insensitive to incident angles from 0° to 60°. For TE wave incidence, the absorptance of the proposed structure is insensitive to incident angles from 0° to 50°. Even if the incident angle reaches 60°, the absorptance is ~90%. This is mainly due to the high symmetry of the proposed structure and the resonant locality of the SP. This property, which is insensitive to the angle of incidence and the direction of polarization, has many practical applications, upon which it has a large effect.

In addition, we also simulated the relationship between the absorption spectrum of the TM and TE incident waves, and the Fermi level, as shown in Figs. 6(a) and 6(b). It can be clearly seen that the proposed structure is not sensitive to the polarization direction of the incident wave, and that the absorption spectrum can be tuned by changing the Fermi level. As the E_f increases, for both the TM wave incidence and the TE wave incidence, both absorption peaks show a shift towards blue, and the absorptance first increases and then decreases. When E_f = 0.8eV, perfect absorption can be reached.
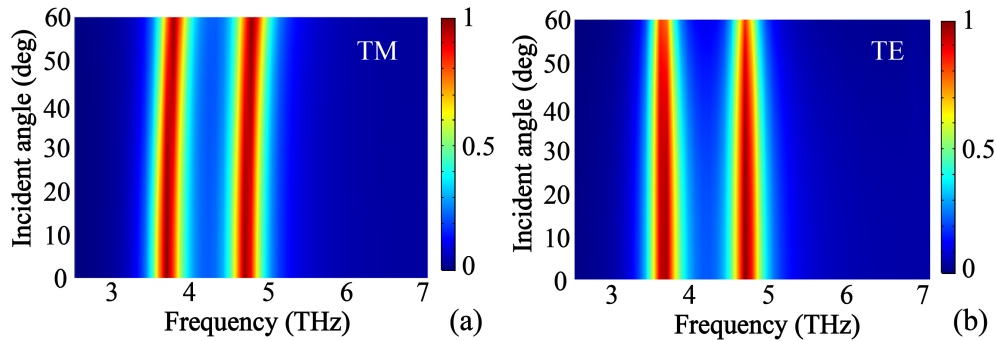

Fig. 5. Absorptance as a function of the incident frequency and the incidence angle, where (a) is the TM wave incident and (b) is the TE wave incident.
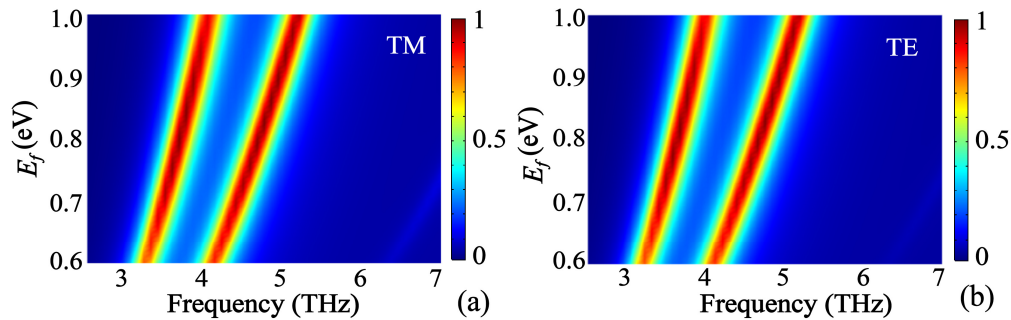

Fig. 6. Absorptance as a function of the incident frequency and Fermi level, where (a) is the TM wave incident and (b) is the TE wave incident.

4. Multi-layer composite structures

Based on the results of the above simulation, we also explored the absorption spectra of the three- and four-layer graphene structure, as shown in Figs. 7 and 8. Figure 7(a) shows a structure with SiO$_2$/graphene/SiC added to the original structure. The thicknesses of newly added SiC and SiO$_2$ are d_1 = 100 nm and d_2 = 200 nm, respectively. The newly added graphene has an outer ring width of p_5 = 580 nm and the inner ring width p_6 = 190 nm. Figure 7(b) is the absorption spectrum of the three-layer graphene structure. Three independent absorption peaks appear. The frequencies corresponding to the absorption peaks are 3.67 THz, 4.75 THz, and 5.81 THz. Although the second absorption peak does not reach perfect absorption, its absorptance is still greater than 98%. The first and third absorption peaks achieve a perfect absorption effect.

Figure 8(a) shows a structure in which a layer of SiC/graphene/SiO$_2$ is further added to the structure in Fig. 7(a), wherein the newly added SiC and SiO$_2$ are of thicknesses d_1 and d_2, respectively. The newly added graphene has an outer ring width of p_7 = 450 nm. The inner ring width is p_8 = 120 nm. Figure 8(b), the absorption spectrum of the four-layer graphene structure, shows the appearance of four independent high absorption peaks and one small absorption

peak. The frequencies corresponding to the absorption peaks are 3.67 THz, 4.73 THz, 5.90 THz, and 6.94THz, respectively. The absorptance of the fourth of the four highest absorption peaks is 98.6% and the remaining absorption peaks are perfectly absorbed.
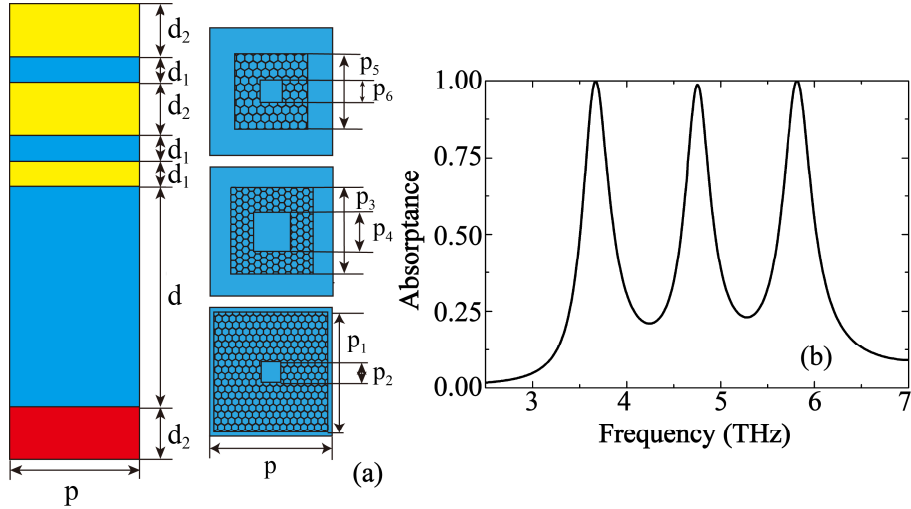

Fig. 7. (a) Side and top views of a three-layer graphene structure with p, p_1, p_2, p_3, p_4 values used. (Fig. 1, $p_5 = 580$nm, $p_6 = 190$ nm.) Each layer of graphene is between SiC and SiO$_2$, and (b) Absorptance spectrum of the three-layer composite structure.

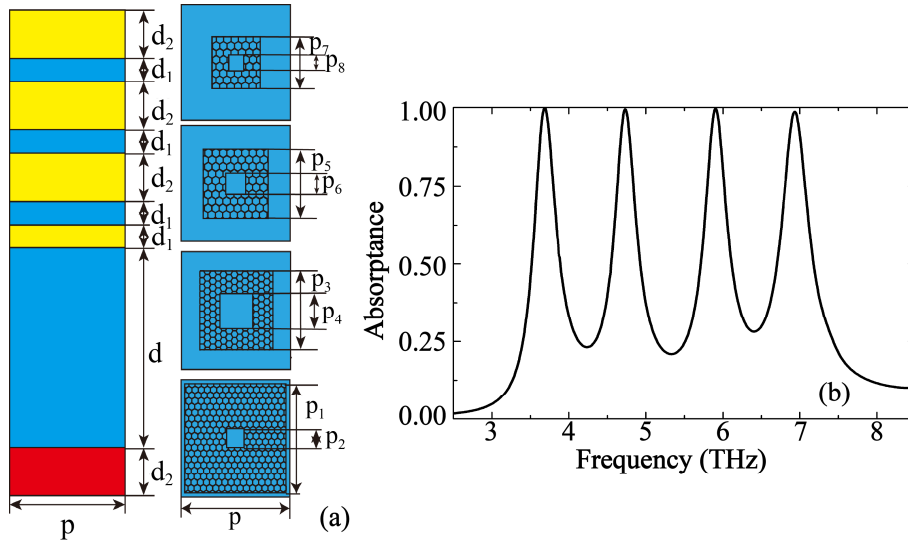
Fig. 8. (a) Side and top views of a four-layer graphene structure with p, p_1, p_2, p_3, p_4 values used. (Fig. 1, $p_5 = 580$ nm, $p_6 = 190$ nm, $p_7 = 450$ nm, $p_8 = 120$ nm.) Each layer of graphene is between SiC and SiO$_2$. (b) Absorption spectrum of a four-layer composite structure.

5. Conclusion

In summary, this paper studied a tunable multi-band perfect absorber in the THz range similar to the multi-layer SiO$_2$/graphene/SiC. We can choose any two desired perfect absorption peaks in a relatively wide THz band by passively adjusting the structural parameters. It is also possible to achieve active coordination of perfect absorption by changing the Fermi level. Due to the structure's high degree of symmetry and the locality of SP resonance, our perfect absorber is insensitive to both the incident angle and the polarization direction. We also

discussed the absorption characteristics of the three-layer structure and the four-layer structure. The simulation results show that up to four perfect absorption peaks can be formed in the THz band. Therefore, we can select the perfect absorption and absorption peaks of the frequency we want in the THz band according to the situation. This strong absorption, the high degree of freedom in selecting the absorption frequency and the diversity of two, three, or four perfect absorption peaks at the same time have an inestimable potential for practical applications.

Funding

References

1. X. Du, I. Skachko, F. Duerr, A. Luican, and E. Y. Andrei, "Fractional quantum Hall effect and insulating phase of Dirac electrons in graphene," Nature **462**(7270), 192–195 (2009).
2. C. Casiraghi, A. Hartschuh, E. Lidorikis, H. Qian, H. Harutyunyan, T. Gokus, K. S. Novoselov, and A. C. Ferrari, "Rayleigh imaging of graphene and graphene layers," Nano Lett. **7**(9), 2711–2717 (2007).
3. A. C. Ferrari, F. Bonaccorso, V. Fal'ko, K. S. Novoselov, S. Roche, P. Bøggild, S. Borini, F. H. Koppens, V. Palermo, N. Pugno, J. A. Garrido, R. Sordan, A. Bianco, L. Ballerini, M. Prato, E. Lidorikis, J. Kivioja, C. Marinelli, T. Ryhänen, A. Morpurgo, J. N. Coleman, V. Nicolosi, L. Colombo, A. Fert, M. Garcia-Hernandez, A. Bachtold, G. F. Schneider, F. Guinea, C. Dekker, M. Barbone, Z. Sun, C. Galiotis, A. N. Grigorenko, G. Konstantatos, A. Kis, M. Katsnelson, L. Vandersypen, A. Loiseau, V. Morandi, D. Neumaier, E. Treossi, V. Pellegrini, M. Polini, A. Tredicucci, G. M. Williams, B. H. Hong, J. H. Ahn, J. M. Kim, H. Zirath, B. J. van Wees, H. van der Zant, L. Occhipinti, A. Di Matteo, I. A. Kinloch, T. Seyller, E. Quesnel, X. Feng, K. Teo, N. Rupesinghe, P. Hakonen, S. R. Neil, Q. Tannock, T. Löfwander, and J. Kinaret, "Science and technology roadmap for graphene, related two-dimensional crystals, and hybrid systems," Nanoscale **7**(11), 4598–4810 (2015).
4. F. Bonaccorso, Z. Sun, T. Hasan, and A. C. Ferrari, "Graphene photonics and optoelectronics," Nat. Photonics **4**(9), 611–622 (2010).
5. F. Xia, H. Wang, D. Xiao, M. Dubey, and A. Ramasubramaniam, "Two-dimensional material nanophotonics," Nat. Photonics **8**(12), 899–907 (2014).
6. F. H. L. Koppens, D. E. Chang, and F. J. García de Abajo, "Graphene Plasmonics: A Platform for Strong Light-Matter Interactions," Nano Lett. **11**(8), 3370–3377 (2011).
7. A. Yu. Nikitin, F. Guinea, F. J. Garcia-Vidal, and L. Martin-Moreno, "Fields radiated by a nanoemitter in a graphene sheet," Phys. Rev. B Condens. Matter Mater. Phys. **84**(19), 195446 (2011).
8. A. Andryieuski and A. V. Lavrinenko, "Graphene metamaterials based tunable terahertz absorber: effective surface conductivity approach," Opt. Express **21**(7), 9144–9155 (2013).
9. P. Y. Chen, C. Argyropoulos, M. Farhat, and J. S. Gomez-Diaz, "Flatland plasmonics and nanophotonics based on graphene and beyond," Nanophotonics **6**(6), 1239–1262 (2017).
10. Z. Sun, A. Martinez, and F. Wang, "Optical modulators with 2D layered materials," Nat. Photonics **10**(4), 227–238 (2016).
11. C. X. Liu, P. G. Liu, C. Yang, Y. Lin, and H. Q. Liu, "Analogue of dual-controlled electromagnetically induced transparency based on a graphene metamaterial," Carbon **142**, 354–362 (2019).
12. S. Y. Xiao, T. Wang, T. T. Liu, X. C. Yan, Z. Li, and C. Xu, "Active modulation of electromagnetically induced transparency analogue in terahertz hybrid metal-graphene metamaterials," Carbon **126**, 271–278 (2018).
13. C. Caucheteur, T. Guo, F. Liu, B. O. Guan, and J. Albert, "Ultrasensitive plasmonic sensing in air using optical fibre spectral combs," Nat. Commun. **7**(1), 13371 (2016).
14. J. Wang, C. Song, J. Hang, Z. D. Hu, and F. Zhang, "Tunable Fano resonance based on grating-coupled and graphene-based Otto configuration," Opt. Express **25**(20), 23880–23892 (2017).
15. J. C. Wang, L. Yang, M. Wang, Z. D. Hu, Q. L. Deng, Y. G. Nie, F. Zhang, and T. Sang, "Perfect absorption and strong magnetic polaritons coupling of graphene-based silicon carbide grating cavity structures," J. Phys. D Appl. Phys. **52**(1), 015101 (2019).
16. C. M. Watts, X. Liu, and W. J. Padilla, "Metamaterial electromagnetic wave absorbers," Adv. Mater. **24**(23), OP98–OP120 (2012).
17. H. A. Atwater and A. Polman, "Plasmonics for improved photovoltaic devices," Nat. Mater. **9**(3), 205–213 (2010).
18. W. W. Salisbury, "Absorbent body for electromagnetic waves," US Patent 2599944 (1952).
19. B. A. Munk, *Frequency Selective Surfaces* (John Wiley and Sons, New York 2000).
20. J. Chen, T. Zhang, C. J. Tang, P. Mao, Y. J. Liu, Y. Yu, and Z. Q. Liu, "Optical Magnetic Field Enhancement via Coupling Magnetic Plasmons to Optical Cavity Modes," IEEE Photonics Technol. Lett. **28**(14), 1529–1532 (2016).

21. J. Chen, C. J. Tang, P. Mao, C. Peng, D. P. Gao, Y. Yu, Q. G. Wang, and L. B. Zhang, "Surface-plasmon-polaritons-assisted enhanced magnetic response at optical frequencies in metamaterials," IEEE Photonics J. **8**(1), 1–7 (2015).
22. K. Aydin, V. E. Ferry, R. M. Briggs, and H. A. Atwater, "Broadband polarization-independent resonant light absorption using ultrathin plasmonic super absorbers," Nat. Commun. **2**(1), 517 (2011).
23. H. Tao, N. I. Landy, C. M. Bingham, X. Zhang, R. D. Averitt, and W. J. Padilla, "A metamaterial absorber for the THz regime: design, fabrication and characterization," Opt. Express **16**(10), 7181–7188 (2008).
24. X. Shen, T. J. Cui, J. Zhao, H. F. Ma, W. X. Jiang, and H. Li, "Polarization-independent wide-angle triple-band metamaterial absorber," Opt. Express **19**(10), 9401–9407 (2011).
25. M. Lei, N. Feng, Q. Wang, Y. Hao, S. Huang, and K. Bi, "Magnetically tunable metamaterial perfect absorber," J. Appl. Phys. **119**(24), 244504 (2016).
26. C. M. Bingham, H. Tao, X. Liu, R. D. Averitt, X. Zhang, and W. J. Padilla, "Planar wallpaper group metamaterials for novel THz applications," Opt. Express **16**(23), 18565–18575 (2008).
27. X. Liu, T. Starr, A. F. Starr, and W. J. Padilla, "Infrared spatial and frequency selective metamaterial with near-unity absorbance," Phys. Rev. Lett. **104**(20), 207403 (2010).
28. R. Xing and S. Jian, "A dual-band THz absorber based on graphene sheet and ribbons," Opt. Laser Technol. **100**, 129–132 (2018).
29. M. Huang, Y. Cheng, Z. Cheng, H. Chen, X. Mao, and R. Gong, "Based on graphene tunable dual-band THz metamaterial absorber with wide-angle," Opt. Commun. **415**, 194–201 (2018).
30. B. Appasani, P. Prince, R. K. Ranjan, N. Gupta, and V. K. Verma, "A simple multi-band metamaterial absorber with combined polarization sensitive and polarization insensitive characteristics for THz applications," Plasmonics **14**(3), 737–742 (2019).
31. Z. Su, J. Yin, and X. Zhao, "Terahertz dual-band metamaterial absorber based on graphene/MgF2 multilayer structures," Opt. Express **23**(2), 1679–1690 (2015).
32. M. P. Fischer, J. Bühler, G. Fitzky, T. Kurihara, S. Eggert, A. Leitenstorfer, and D. Brida, "Coherent field transients below 15 THz from phase-matched difference frequency generation in 4H-SiC," Opt. Lett. **42**(14), 2687–2690 (2017).
33. X. H. Deng, J. T. Liu, J. Yuan, T. B. Wang, and N. H. Liu, "Tunable THz absorption in graphene-based heterostructures," Opt. Express **22**(24), 30177–30183 (2014).
34. E. H. Hwang and S. Das Sarma, "Dielectric function, screening, and plasmons in two-dimensional graphene," Phys. Rev. B Condens. Matter Mater. Phys. **75**(20), 205418 (2007).
35. L. A. Falkovsky and S. S. Pershoguba, "Optical far-infrared properties of a graphene monolayer and multilayer," Phys. Rev. B Condens. Matter Mater. Phys. **76**(15), 153410 (2007).
36. G. W. Hanson, "Dyadic Green's functions and guided surface waves for a surface conductivity model of graphene," J. Appl. Phys. **103**(6), 064302 (2008).
37. S. Xiao, T. Wang, Y. Liu, C. Xu, X. Han, and X. Yan, "Tunable light trapping and absorption enhancement with graphene ring arrays," Phys. Chem. Chem. Phys. **18**(38), 26661–26669 (2016).
38. S. Ke, B. Wang, H. Huang, H. Long, K. Wang, and P. Lu, "Plasmonic absorption enhancement in periodic cross-shaped graphene arrays," Opt. Express **23**(7), 8888–8900 (2015).
39. G. Yao, F. Ling, J. Yue, C. Luo, Q. Luo, and J. Yao, "Dynamically electrically tunable broadband absorber based on graphene analog of electromagnetically induced transparency," IEEE Photonics J. **8**(1), 7800808 (2016).
40. K. S. Novoselov, A. K. Geim, S. V. Morozov, D. Jiang, Y. Zhang, S. V. Dubonos, I. V. Grigorieva, and A. A. Firsov, "Electric field effect in atomically thin carbon films," Science **306**(5696), 666–669 (2004).
41. A. K. Geim and K. S. Novoselov, "The rise of graphene," Nat. Mater. **6**(3), 183–191 (2007).
42. A. Yariv, "Coupled-mode theory for guided-wave optics," IEEE J. Quantum Electron. **9**(9), 919–933 (1973).
43. H. Xu, H. Li, Z. He, Z. Chen, M. Zheng, and M. Zhao, "Dual tunable plasmon-induced transparency based on silicon-air grating coupled graphene structure in THz metamaterial," Opt. Express **25**(17), 20780–20790 (2017).